

# TRIAXIAL RESIDUAL STRESSES AFFECT DRIVING FORCE AND CONSTRAINT TO ALTER FRACTURE TOUGHNESS

Michael R. Hill and Theodore Yau  
Mechanical and Aeronautical Engineering  
University of California  
One Shields Avenue, Davis, CA 95616, USA

## ABSTRACT

This paper discusses the role of triaxial residual stresses in altering fracture behavior. Historically, residual stress effects in fracture have focused on the crack driving force, so that opening mode residual stresses are assumed solely to influence fracture. However, residual stresses can also impact constraint conditions at the crack-tip, thereby altering effective material toughness. This paper illustrates these two residual stress effects by discussing recent numerical and experimental results. The numerical aspects of the paper employ non-linear finite element analyses in which residual stresses are handled using eigenstrain. Micromechanical fracture prediction schemes, which depend directly on the crack-tip conditions rather than a global parameter, are used to predict fracture. Domain integral solutions for the crack driving force, derived from FEM results, allow comparison between the micromechanical and more traditional global parameter approaches. Experimental toughness measurements from notched bend bars containing triaxial residual stresses due to local compression complement the numerical work by demonstrating the accuracy of the micromechanical approach. Finally, discussions highlight the need to consider both the driving force and constraint effects caused by residual stresses when predicting structural failure.

## 1 INTRODUCTION

Recent research in micromechanical modeling has made progress toward the accurate prediction of fracture under various crack-tip constraint conditions. Historically, fracture prediction has focused on determining a global fracture parameter (e.g., the  $J$ -integral,  $J$ , or the Mode-I stress intensity factor,  $K_I$ ) as a function of applied load, and finding the load at which the parameter exceeds a critical level for fracture. This approach rests on the assumption that the fracture parameter alone controls the crack-tip stress and strain. Unfortunately, in application, material non-linearity (i.e., yielding) at the crack-tip invalidates this assumption. Yielding is a function of the triaxial state of stress, and the crack-tip stress state has a range of variation in real structures. In fact, it is well known that differences in crack-tip triaxiality (or, more commonly "constraint") can exist in structures due to differences in geometry and applied loading (e.g., thick versus thin, or tension versus bending). Further, different crack-tip stresses lead to fracture at different levels of the global fracture parameter. An alternative method to parameter-based approaches, micromechanical methods directly examine the crack-tip stress and strain state to provide an estimate of fracture propensity. Implementation of the micromechanical approach therefore requires the prediction of crack-tip stress and strain, and its history with applied loading. In practice, finite element methods (FEM) are used to compute the crack-tip conditions, as a function of applied loading.

Application of the micromechanical approach to predict fracture in residual stress bearing structures provides some surprising results. The traditional approach to predict fracture of residual stress (RS) bearing, flawed components involves linear superposition. This approach assumes that only opening mode RS will impact the fracture process, when, in fact, residual

stresses are often triaxial. Triaxial RS will influence non-linear material behavior at the crack-tip, a process not accounted for by superposition. Including RS in a micromechanical approach, however, does allow the residual stress field to affect the behavior of material at the crack-tip. Accordingly, the micromechanical approach offers a more complete accounting of RS effects in fracture, and gives insight to the fracture process when RS is present.

This paper explains the application of micromechanics when RS is present, and illustrates the significance of RS-induced constraint.

## 2 FRAMEWORK

This section describes a computational and analytical framework for predicting fracture in flawed, RS bearing structures using micromechanics. We first lay out the general finite element procedures employed. Next, we describe methods for introducing RS into the computation. The computational results provide the crack-tip stress and strain history as a function of applied load, which serve as input to a micromechanical fracture prediction model. Two such models for predicting fracture are presented: the RKR model for brittle fracture, and the SMCS model for ductile fracture. Finally,  $J-Q$  analysis is described, which helps to interpret the stress and strain history at the crack-tip, and to compare the results of micromechanics to those that would be obtained using a traditional global parameter approach.

### 2.1 General analysis techniques

Elastic-plastic finite element computation is used to simulate the response of a structure of interest to both applied and residual stresses simultaneously. The finite element solutions employ a non-linear, finite strain formulation. Plasticity is assumed to follow isotropic, incremental  $J_2$  flow theory with a piece-wise linear Cauchy-stress logarithmic-strain curve obtained from tensile testing. Commercial codes can be used to perform these analyses. Mesh refinement in the crack-tip region is critical, and must assure that stress and strain are accurately captured in the near crack-tip region. Time-stepping in the analysis provides a means to capture the developing crack-tip state with increasing applied load.

### 2.2 Inclusion of residual stress

Residual stress is included in the finite element computation using eigenstrain. Eigenstrain is a combination of all the non-elastic, incompatible strains set up during processing of a material Mura (1). In welding, the eigenstrain is a combination of thermal, plastic, and transformation strains; in coining or autofrettage, the eigenstrain is due to plasticity. The eigenstrain field is defined with reference to elastic deformation of the structure, and reproduces the entire RS state when the material behavior is elastic. For a particular process the eigenstrain field is a tensor with spatial dependence, and can be found experimentally Hill (2) or by modeling Goldak (3).

The use of an eigenstrain distribution in modeling offers several advantages for further analysis. First, the residual stress present can be determined by imposing the eigenstrain distribution in a linear elastic finite element model of the geometry. (Note that residual stresses, by their nature, do not result in active yielding, and a valid eigenstrain field must impose stresses that satisfy the yield criterion). Although an eigenstrain analysis is complicated by the spatial variation of each component of the eigenstrain tensor, a general-purpose finite element program can be used to produce the RS field. Further, when the eigenstrain field is known, the entire, full-field, triaxial RS state is known at every point within the structure.

When the eigenstrain field is known for the unflawed structure, the analysis of a flawed structure can be performed. The addition of a crack introduces new surfaces, and the RS state in the flawed body depends on these surfaces. If the structure is linear elastic, the state is found simply by modeling the traction-free surfaces. In non-linear materials, crack-tip

yielding must be allowed when introducing the flaw. To handle this situation, the eigenstrain distribution is first imposed in the body with crack-face nodes restrained, and the equilibrium RS state found (this step is elastic). Then, the crack-face nodes are released in succession, so that the crack gradually extends from the free surface to simulate fatigue (this step can be elastic-plastic). The rate at which the crack is extended will have a bearing on the crack-tip fields, and one must ensure that the opening is gradual enough (e.g., so subsequent fracture analysis is not affected). When properly executed, this process redistributes the original RS field, allowing for crack-tip yielding, and resulting in a flawed RS bearing structure.

Once RS is introduced into the computation, applied loading is simulated. During this subsequent loading phase, the residual and applied stresses act together at the material level. Any new plastic deformation is the result of both stress types. Therefore, this analysis technique allows for the non-linear interaction of RS and applied loading, which is not accounted for when applying global approaches.

An alternative to using eigenstrain is to directly simulate the process causing the RS field. Results of this simulation can then be used as initial conditions for the simulation of applied loading. However, direct simulation can only be readily pursued for simple problems, with small amounts of plasticity or other non-linear strain.

### 2.3 Micromechanical fracture prediction

Since the analysis technique just described provides a complete description of the material state in the presence of residual and applied loading, the crack-tip material history can be used within a micromechanical scheme to predict fracture. The physical phenomena occurring in the fracture process vary, and it is generally useful to consider brittle and ductile fracture processes separately Shih (4). Here we briefly describe one model for predicting each type of fracture. In principle, other micromechanical models could be employed.

#### 2.3.1 The RKR model for cleavage fracture initiation

Initiation of cleavage fracture in mild steels can be predicted using the RKR micromechanical model Ritchie (5). This simple model predicts fracture when the opening stress,  $\sigma_{yy}$ , ahead of the crack-tip exceeds a fracture stress,  $\sigma_f^*$ , over a microstructurally relevant distance,  $l^*$ . In applying this model, one monitors the progress of the opening stress ahead of the crack-tip due to residual and applied loading. Once the RKR criterion is satisfied, fracture is predicted. The parameters in the RKR model are typically found through laboratory testing for a given material and reported ranges for steels are 2 to 5 grain diameters for  $l^*$ , and 2 to 4 times the yield strength for  $\sigma_f^*$  Ritchie (5). When the micromechanics condition for fracture initiation is satisfied, the associated applied load and global fracture parameters (e.g.,  $J$ -integral) can be found from the FEM results.

#### 2.3.2 The SMCS model for ductile fracture initiation

Ductile fracture behavior is dependent upon both the stress and deformation state at the crack-tip. The micro-mechanisms of ductile fracture are void nucleation and growth, both of which precipitate from second-phase particles within the microstructure. Local plastic strain and hydrostatic stress drive the nucleation and growth process. Mackenzie, et al., proposed a model which predicts the initiation of ductile fracture when equivalent plastic strain near the crack-tip,  $\epsilon'_p(r, \theta)$ , exceeds a critical amount,  $\epsilon_p^{crit}(r, \theta)$ , over some distance ahead of the crack-tip,  $l_d^*$  (where  $r$  and  $\theta$  are crack-tip centered coordinates) MacKenzie (6). This critical level of plastic strain depends on the ratio of hydrostatic to von Mises stress at a given material point,  $\bar{\sigma}/\sigma'$ . The characteristic length,  $l_d^*$ , is related to the spacing of second-phase particles. The critical level of plastic strain can be written for many materials as Rice (7)

$$\epsilon_p^{crit}(r, \theta) = \alpha \exp\left(-\beta \frac{\bar{\sigma}(r, \theta)}{\sigma'(r, \theta)}\right) \quad [1]$$

Here,  $\alpha$  and  $\beta$  are material parameters, fitted to data obtained from tests and analyses of notched tensile specimens MacKenzie (6). To predict fracture initiation, one can compute the parameter

$$\text{SMCS}(r, \theta) = \varepsilon'_p(r, \theta) - \varepsilon_p^{\text{crit}}(r, \theta) \quad [2]$$

where SMCS reflects the common name for this method: stress-modified critical strain Panontin (8). For a given loading condition, fracture is predicted when

$$\text{SMCS}(r, \theta) \geq 0 \text{ for all points } r \leq l_d^*, \theta = \bar{\theta} \quad [3]$$

In this expression it is recognized that ductile fracture will not necessarily initiate directly ahead of the crack-tip, but possibly at an oblique angle,  $\theta = \bar{\theta}$ . In application,  $\bar{\theta}$  is found by maximizing SMCS with  $\theta$  for  $r = l_d^*$ .

## 2.4 Characterization of crack-tip behavior

When the above procedures are used to predict fracture, none of the traditional global fracture parameters are used. Nevertheless, it is useful to compare the micromechanical predictions with those that might be made using a traditional approach. To perform this comparison, we utilize two parameters, one related to driving force and one to constraint. Specifically, we invoke  $J$ - $Q$  theory, which was developed from simulation of crack-tip fields in finite and infinite size bodies O'Dowd (9), O'Dowd (10).

During the non-linear analysis, the  $J$ -integral is estimated at each increment of applied loading using the domain-integral technique. As such, the computed value of  $J$  includes the contribution of residual stress within the material. For a given level of  $J$ , the constraint conditions at the crack-tip are represented by the parameter  $Q$ .  $Q$  has been shown to characterize the magnitude of the hydrostatic stress over the forward sector ahead of the crack-tip to a good approximation.  $Q$  is formally defined as

$$Q = \frac{\sigma_{\theta\theta} - \sigma_{\theta\theta}^{\text{ssy}}}{\sigma_o} \text{ at } \theta = 0, r/(J/\sigma_o) = n \quad [4]$$

where,  $\sigma_o$  is the material yield strength, and  $n$  is a constant, usually taken in the range 2 to 4 O'Dowd (9), O'Dowd (10).  $Q$  depends on the crack-tip stress state in the body of interest,  $\sigma_{\theta\theta}$ , and on the stress state in a plane-strain, Mode I loaded, small-scale yielding reference solution,  $\sigma_{\theta\theta}^{\text{ssy}}$ , where both are subject to the same applied  $J$ .

Because  $Q$  is a constraint parameter, it provides insight into the fracture process.  $Q$  near zero suggests that a body is in small-scale yielding. As deformation levels increase in finite specimens, the hydrostatic stresses at the crack-tip are relieved, producing a negative  $Q$  value, and signaling a loss in constraint. A negative value of  $Q$  indicates lower crack-tip stress compared to a body in small-scale yielding and, therefore, a reduced propensity for cleavage fracture at a given value of  $J$ . A positive  $Q$ -value indicates that high constraint exists for a particular crack-tip state.

Having the above framework at hand, we employ it in two examples, one purely computational, and one a hybrid of computation and experiment. These two examples illustrate the method and bring up some interesting results for discussion.

## 3 TRIAXIAL STRESS EFFECTS IN BRITTLE FRACTURE

This section summarizes a recent numerical study on the influence of RS on brittle fracture of a welded mild steel structure. The RKR micromechanical model is used to predict fracture. Details of the study can be found in Panontin (11).

### 3.1 Geometry and material

This section focuses on the prediction of brittle fracture of the axially loaded, girth-welded

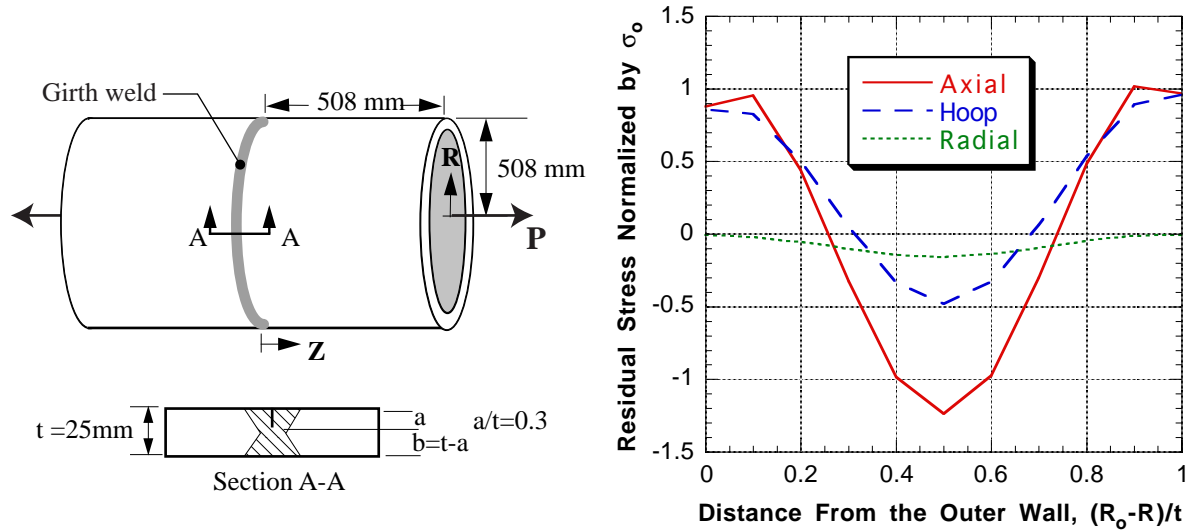


Figure 1 – (a) Girth-welded pressure shell, (b) RS in the unflawed condition

shell shown in Figure 1(a), initiating from a circumferential external flaw. The properties assumed are those of A516-70, a high hardening, ferritic, pressure vessel steel with uniaxial yield strength of 303 MPa. The RKR parameters for this material are assumed to be  $\sigma_j^* = 3.5\sigma_0$  and  $l^* = 0.15$  mm, or about 3 ferritic grain diameters.

### 3.2 Residual stresses

This analysis makes use of an assumed eigenstrain distribution. This distribution gives rise to residual stresses that are typical of a continuously welded, double-sided joint in mild steel plate Gunnert (12). The nature of continuous welding allows the assumption of an eigenstrain field that depends on the transverse and through-thickness welding directions, but is independent of position along the weld. Further, the eigenstrain field is assumed symmetric about both the centerline of the weld and the mid-wall of the shell. The residual stress field computed when the assumed eigenstrain field is imposed in the un-flawed geometry is shown in Figure 1(b), on the plane where the crack will be introduced. For the flaw orientation shown in Figure 1(a), axial stresses correspond to the opening mode, and over the length of defect considered (from 0 to 0.3 in Figure 1(b)), the axial RS is tensile. Accordingly, RS will tend to increase the crack-driving force and therefore decrease the fracture load.

### 3.3 Results

Fracture predictions using the RKR model show a strong constraint effect caused by RS. Fracture loads are predicted to be 21.3 MN and 9.83 MN without and with RS, respectively. Because RKR is satisfied at these loads, crack-tip opening stresses are nearly the same in each different geometry. However, this occurs at markedly different values of  $J$ , 36.7 kN/m without RS and 13.5 kN/m with RS. Recall that these values of  $J$  are computed using the domain integral, so they include the influence of RS on driving force. As shown in Figure 2(a), the significant change in  $J$  at fracture is due to high constraint imposed by the RS field. Figure 2(b) shows that this additional constraint suppresses plastic strain formation compared with the non-residual stress bearing case. These interesting results demonstrate that RS can cause a significant change in crack-tip constraint. Figure 2(a) shows clearly that the tension loaded shell has quite low constraint when RS is absent, but behaves like a body in small-scale yield when RS is present. If the RS bearing shell were assumed to have constraint similar to the RS-free shell, the superposition approach would lead to an erroneous and non-conservative fracture assessment. This observation gives credence to codified assumptions of high constraint, as RS can combine with applied loads to produce highly constrained crack-

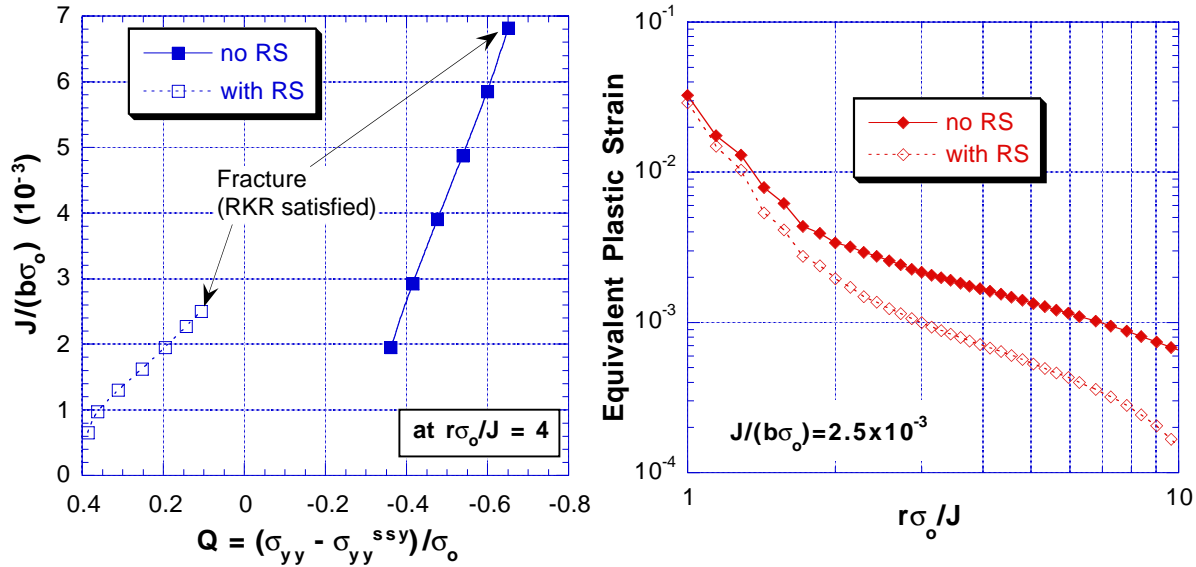


Figure 2 - (a) J-Q trajectories and (b) plastic strain for the shell

tip fields in a geometry and loading condition that would otherwise exhibit low constraint.

#### 4 TRIAXIAL STRESS EFFECTS IN DUCTILE FRACTURE

This section discusses an experimental and computational investigation of residual stress effects on ductile fracture initiation in a high strength aluminum alloy. Residual stresses are introduced by local compression near the crack-tip. Results show that fracture predictions performed using the SMCS criterion predict the experimental trend of decreasing toughness with increasing local compression.

##### 4.1 Geometry and material

A standard SE(B) specimen geometry is used, loaded in three point bending as shown in Figure 3(a). Experimental toughness measurements are made under various conditions. Two specimen thicknesses are used, corresponding to half- and full-plate thickness (12.5 and 25 mm). Nominal planar dimensions of these two specimen types were fixed at  $W = 25$  mm and  $S/W = 4$ .

All specimens were removed in the TL orientation from a single 25 mm thick 7050 T7451 aluminum plate. 7050 is a high strength alloy resistant to stress corrosion cracking. It has low hardening ( $n \approx 17$ ), with a uniaxial yield strength of 531 Mpa (determined experimentally). The micromechanisms of fracture are ductile, although occurring at low energy. SMCS parameters found for this material in a previous study are:  $\alpha = 4.2$ ,  $\beta = 3.7$ , and  $l_d^* = 0.15$  mm Hill (13).

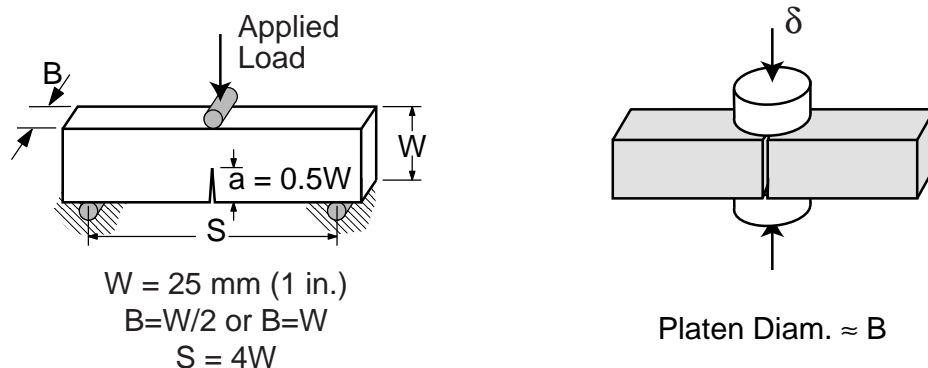


Figure 3 - (a) SE(B) geometry employed, (b) illustration of local compression

## 4.2 Residual stresses

Residual stresses are introduced into fracture specimens by local compression (LC). That is, two cylindrical platens are used to make indentations on both sides of the specimen on the W-S face, near the crack tip, as shown in Figure 3(b). LC is normally used to relieve weld residual stresses to allow fracture testing Towers (14), but it obviously produces its own triaxial RS field Hill (15). The amount of LC is usually stated as the permanent thickness reduction divided by original thickness, in percent. LC is relatively simple to perform and well controlled. In this study, LC provided a repeatable RS state, whose subsequent effect on fracture could be assessed.

Experimentally, full thickness (BxB) specimens were compressed about 1% using a 20 mm platen, and half-thickness (Bx2B) specimens were compressed from 1.2 to 2.5% using a 12 mm platen. LC was performed on notched SE(B)'s, prior to fatigue pre-cracking.

Computationally, residual stresses are included by direct simulation. That is, four steps were included in the FEM analysis. First, local compression was simulated by modeling the compression platen as a rigid body, in frictionless contact with the SE(B) specimen, and applying to it a given deformation. Second, the compression load was removed and the RS state obtained. Third, the crack was extended by node release to simulate pre-cracking. Finally, three-point loading was simulated. Results during this final step were used with the SMCS criterion to predict fracture. SMCS parameters are assumed independent of the LC process. That assumption is only valid over a small range of compression, as increasing plastic deformation will eventually alter microstructure and influence the fracture process.

## 4.3 Experimental procedures

Specimens were tested on a computer controlled, servo-hydraulic test frame, following procedures in ASTM E813. Digitally acquired load and mouth-opening data were reduced according to ASTM E399 to provide values of candidate initiation toughness,  $K_Q$ .

## 4.4 Results

Experimental results are plotted in Figure 4(a), showing the effect of LC on measured toughness. For the Bx2B specimens, LC reduces measured toughness about 6.7% per percent of LC applied. For the BxB specimen, LC has a greater effect and reduces toughness by about 17% per percent LC.

Computational results shown in Figure 4(a) agree with the experimental trends, but over-predict the effect of LC. The micromechanical approach predicts a toughness drop of 9.1% per percent LC applied for Bx2B specimens, and 23% for the BxB specimens.

The computational results allow insight into the reason for the toughness decrease caused by LC.  $J$ - $Q$  results for three SE(B) specimen conditions discussed above are shown in Figure 4(b). Here we see that RS due to LC increases crack-tip stresses at a given  $J$ . The thicker specimens are subject to a higher degree of additional constraint at a lower level of LC. However, SMCS predicts fracture at roughly the same  $J$  in each specimen type, which suggests that the SMCS predictions are not highly dependent on the initial constraint conditions. (For reference, results of a simulation for a shallow crack specimen, with  $a/W = 0.15$ , are also shown in Figure 4(b). These show that SMCS predicts a large toughness change for a similar magnitude, but opposite sign, constraint change.) The toughness drop shown in Figure 4(a), then, must be due mainly to driving force, not constraint, especially for the thick specimen. This comparison of the RS effects on driving force and constraint in fracture can only be accomplished with the type of modeling discussed here. Therefore, these results demonstrate the usefulness of micromechanical modeling when considering fracture in RS-bearing structures. Further, the approach discussed here provides fracture predictions in good agreement with experimental results.

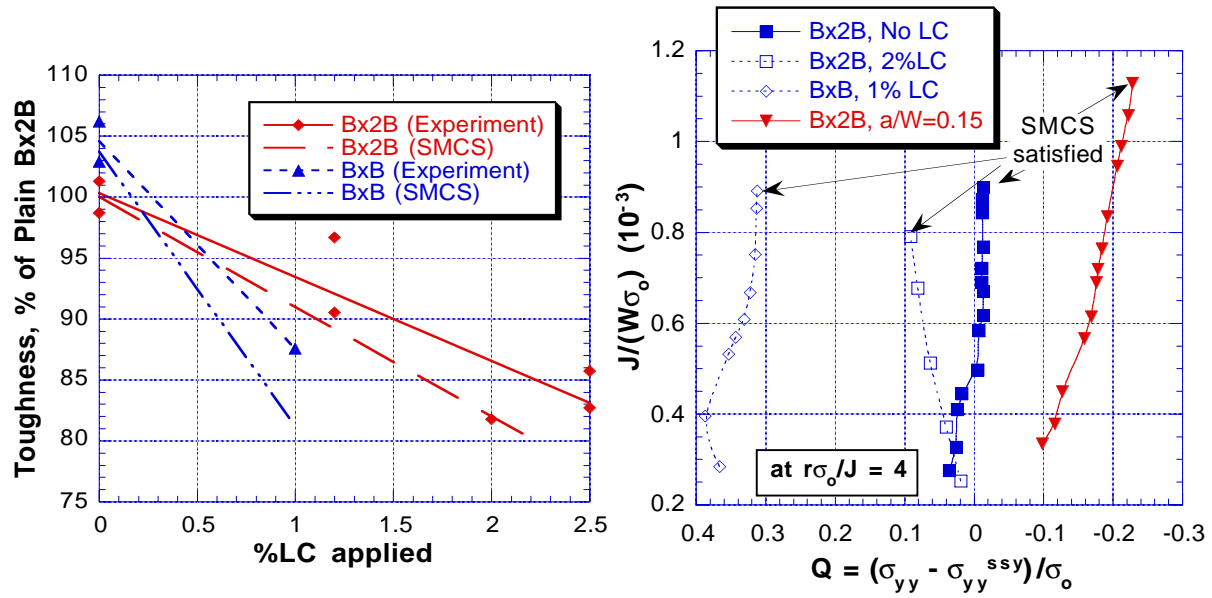


Figure 4 - The effect of LC: (a) Measured toughness, and (b) J-Q trend

## 5 DISCUSSION

This paper is intended to stimulate discussion regarding accepted methods of accounting for residual stresses in fracture prediction. Both computational and experimental results suggest a more thorough assessment of residual stress should be pursued, especially when the RS field is triaxial. Brevity here requires only a brief coverage of the requisite topics, and the interested reader should consult the references provided below.

## 6 REFERENCES

1. Mura T, 'Micromechanics of Defects in Solids', M. Nihoff (Dordrecht, Netherlands), 1987
2. Hill M R, 'Determination of Residual Stress Based on the Estimation of Eigenstrain', Ph.D. Thesis, Stanford University (1996)
3. Goldak J A, Patel B, et al, Adv Joining of Materials (AGARD CP-398) (1985) 1
4. Shih C F, Fat and Fract Mech, 29th Vol, ASTM STP 1332 (1999) 9
5. Ritchie R O, Server W L, Wullarert R A, Met Trans A 10 (1979) 1557
6. MacKenzie A C, Hancock J W, Brown D K, Eng Fract Mech 9 (1977) 167
7. Rice J R, Tracey D M, J Mech Phys Solids 17 (1969) 201
8. Panontin T L, Sheppard S D, Fat and Fract Mech, 26th Vol, ASTM STP 1256 (1995) 54
9. O'Dowd N P, Shih C F, J Mech Phys Solids 39 (1991) 989
10. O'Dowd N P, Shih C F, J Mech Phys Solids 40 (1992) 939
11. Panontin T L, Hill M R, Int J Fract 82 (1996) 317
12. Gunnert R, Proceedings of the Special Symposium on the Behavior of Welded Structures (1961) 164
13. Hill M R, Panontin T L, Manuscript in preparation for submission to Engineering Fracture Mechanics
14. Towers O L, Dawes M G, Elastic-Plastic Fracture Test Methods: The Users' Experience, ASTM STP 856 (1985) 23
15. Hill M R, Panontin T L, Fat and Fract Mech, 29th Vol, ASTM STP 1332 (1999) 154